Millisecond Ordering of Block Copolymer Films *via* Photothermal Gradients

Pawel W. Majewski and Kevin G. Yager*

Center for Functional Nanomaterials, Brookhaven National Laboratory, Upton, New York 11973, United States

ABSTRACT For the promise of self-assembly to be realized, processing techniques must be developed that simultaneously enable control of the nanoscale morphology, rapid assembly, and, ideally, the ability to pattern the nanostructure. Here, we demonstrate how photothermal gradients can be used to control the ordering of block copolymer thin films. Highly localized laser heating leads to intense thermal gradients, which induce a thermophoretic force on morphological defects. This increases the ordering kinetics by at least 3 orders of magnitude compared to conventional oven annealing. By simultaneously exploiting the thermal gradients to induce shear fields, we demonstrate uniaxial alignment of a block copolymer film in less than a second. Finally, we provide examples of how control of the incident light field can be used to generate prescribed configurations of block copolymer nanoscale patterns.

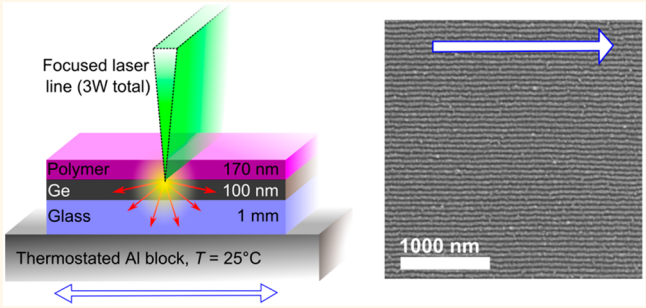

KEYWORDS: laser zone annealing · block copolymers · directed self-assembly · coarsening kinetics · thermophoresis

The promise of self-assembly lies in the spontaneous and intrinsically parallelized ordering, yielding macroscopic materials with nanoscale precision and prescribed functionality. Block copolymers (BCPs) are a particularly well-studied self-assembly motif, wherein chemically distinct blocks of a polymer architecture lead to microphase separation, forming a nanoscale morphology with well-defined periodicity. This powerful paradigm has already demonstrated its potential for the formation of bulk materials,[1] ordered thin films,[2] and functional templates.[3] Despite the enormous potential, self-assembling thin films have seen comparatively little uptake in commercial applications, owing to substantial outstanding challenges: (1) the morphology and orientation of the nanodomains must be controlled; (2) especially for device architectures, the nanodomains must be *patterned*, ideally with macroscopic registry and prescribed spatial distribution; (3) the typical thermal annealing times for achieving reasonable order in self-assembling systems are often impractically long for industrial viability.

A wide range of novel studies have addressed these challenges. The orientation of BCP domains can be controlled *via* processing conditions (*e.g.*, the interplay of temperature and film thickness[4]), substrate surface energy[5−7] and topography,[8−10] electric[11,12] or magnetic[13] fields, or shear.[14−17] The patterning of BCPs has been accomplished by using topographic[18−20] and chemical[21,22] templates in order to locally direct morphology,[23] where it has been shown that density multiplication[24,25] is possible and that minimal design rules can enforce arbitrary nanoscale patterns.[26,27] Block copolymer assembly kinetics have been enhanced through the use of templating,[28] interfacial energy,[29] solvent annealing,[30−32] and microwave annealing.[33] Thermal zone annealing[34]—sweeping a localized hot region through a material to improve order—has been applied to organic materials[35] and recently to block copolymers,[36,37] where improved ordering kinetics, compared to conventional oven annealing, were observed.[38] In the so-called "cold zone annealing" (CZA) implementation, the maximum annealing temperature is well below the order-to-disorder

* Address correspondence to kyager@bnl.gov.

Received for review December 16, 2014 and accepted March 12, 2015.

Published online March 12, 2015
10.1021/nn5071827

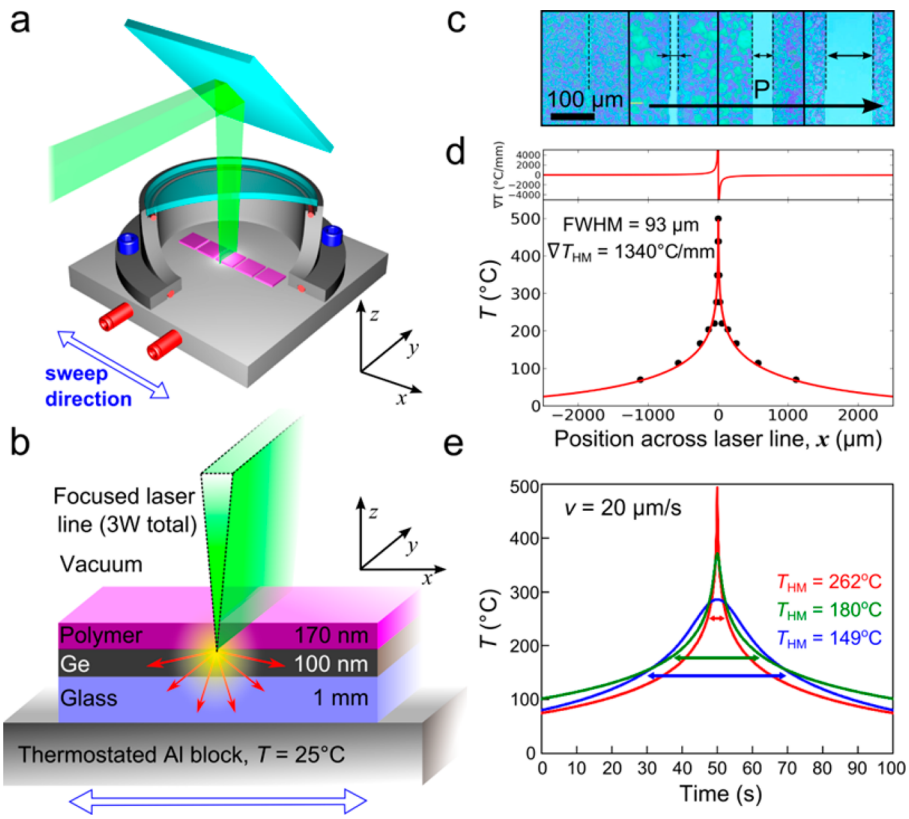

Figure 1. Overview of laser zone annealing (LZA). (a) Cutaway view of the vacuum chamber mounted on a motorized stage, loaded with a set of substrates under laser illumination (laser line shown in green). (b) Schematic of a typical sample: light absorption by a layer of germanium underlying a block copolymer film induces heating (yellow). The thermal profile is determined by the laser line and conduction (red arrows). (c, d) Surface temperature profiling: (c) a series of *melt-marks* inscribed in a thin film of thermometric substance (TBAHFP), as a function of increasing laser power. The contours represent isotherms from which we reconstruct the thermal distribution. (d) Reconstructed surface temperature profile of a 100 nm Ge coated glass slide (across the laser line), showing both experimental isotherms (black dots) and a fit to an analytical function (red curve). The corresponding thermal gradient is plotted above. (e) Reconstructed thermal profiles for different laser focusing. The data have been rescaled into the time domain (for a 20 μm/s sweep speed) in order to emphasize the temporal processing history (time = 0 is arbitrary).

transition temperature. Ordering is thus occurring on both the heating and cooling fronts, through an accelerated annealing process, which is qualitatively different from directional solidification.[39,40] The origin of the enhanced kinetics of CZA was tentatively ascribed to the in-plane thermal gradients,[41] which are on the order of 10−70 °C/mm.

Despite this immense progress in controlling the assembly of BCPs, it remains difficult to formulate a single processing protocol that simultaneously addresses all of the above-enumerated challenges. Herein, we demonstrate the use of laser illumination to generate highly localized thermal fields within a block copolymer thin film. The immense thermal gradients, coupled to high peak temperatures, yield a massive kinetic enhancement with respect to conventional oven annealing. Moreover, the use of a laser as a directing field provides unprecedented control over the assembly process. Photothermal annealing enables robust control of thermal history, allowing tuning of morphology and orientation (both in-plane and out-of-plane). Simultaneously, the use of light as a heat source offers a substantial advantage: optical masking allows annealing to be performed in a spatially controlled way, allowing direct patterning of the BCP morphology *via* the incident light field. Thus, our photothermal gradient method provides a path toward simultaneously addressing the three challenges outlined above.

Laser illumination has been applied to a variety of material-processing protocols, including ordering intrinsically photoresponsive materials,[42] heating inorganic and semiconducting materials, and, more recently, annealing polymeric materials including photoresists[43,44] and during solvent annealing of block copolymers.[45] What we demonstrate here is that careful control of a sweeping laser line enables tuning of the spatiotemporal thermal gradient, providing a precise and powerful method for exploiting the directed ordering effects of zone annealing. This allows for rapid ordering and alignment of samples over macroscopic areas.

RESULTS AND DISCUSSION

Figure 1a shows the laser zone annealing (LZA) setup we constructed to enable localized heating of

polymer thin films. A high-power (3 W) green (532 nm) laser beam is focused into a sharp line and reflected toward samples within a vacuum enclosure. The enclosure is mounted to a linear translation stage, allowing the samples to be swept through the focused laser line (the illuminated area is ~20 μm by >20 mm). We induce local photothermal heating of the polymer samples through the use of specially designed substrates (Figure 1b): a thin germanium coating (50−300 nm) is used as a light-absorbing layer, deposited onto a glass substrate (whose relatively low thermal conductivity enables larger thermal gradients to be established). The laser line is locally absorbed by the Ge layer, giving rise to a thermal field that locally anneals the BCP film cast atop. This setup provides detailed control over the annealing conditions: the temperature scale can be adjusted by laser power and/or Ge thickness, the thermal gradient can be controlled by the laser focus, the dynamic annealing history can be controlled by the sample motion through the laser line, and, more generally, the detailed thermal field can be controlled by shaping the incident light field.

We assessed the local temperature distribution within our nanoscale thin films using a novel phase-change thermometry method (Figure 1c,d; refer to the Supporting Information, SI, for details). As can be seen in Figure 1e, defocusing the laser leads to a correspondingly broader temperature distribution; that is, the thermal distribution can be optically prescribed. There is a limit to the sharpness of the thermal zone, because the thermal field becomes dominated by the intrinsic thermal diffusivity of the substrate. For the glass substrates considered here (thermal diffusivity 0.517 mm^2/s), the sharpest possible thermal zone has a fwhm = 76 μm. Because zone annealing imposes a nontrivial thermal history, there can be no single definition of the effective annealing temperature or time. We note that the maximum temperature of the thermal profile is maintained in the film only for a vanishingly short time (owing to the sweeping of the thermal zone) and is thus not the most meaningful measure of processing. We thus characterize the thermal profile by T_{HM}, the temperature at the half-maximum of the thermal excess. We similarly characterize the typical thermal gradient of a given profile using ∇T_{HM}, the gradient at the half-maximum position along the thermal curve, while noting that the gradient varies throughout the thermal profile. For the sharpest (76 μm) thermal zone with T_{HM} = 274 °C, we obtain ∇T_{HM} = 1790 °C/mm, with a maximum thermal gradient greater than 4000 °C/mm. We similarly refer to t_{HM}—the time the film is above T_{HM}—as the "residence time" and use this as an effective annealing time. Although this definition is arbitrary, we note that because of the extreme sharpness of the hot zone, alternate definitions of the effective annealing time (*e.g.*, the total time above T_g) would be within a small multiple of t_{HM} and would not appreciably affect our conclusions. The total residence time can be conveniently varied by adjusting the LZA sweep velocity and/or by performing repeated sweeps of the sample through the narrow hot zone.

Figure 2 shows results for annealing of a cylinder-forming polystyrene-*b*-poly(methyl methacrylate) thin film (170 nm); this material has a repeat spacing (cylinder-to-cylinder distance) of 31 nm. Conventional oven annealing for 1 h yields a mixed morphology of horizontally and vertically oriented cylinders, as evidenced by the coexistence of fingerprint/line patterns and hexagonal/dot patterns, respectively. At this film thickness, we do not observe any surface terracing ("islands and holes"), which can occur when film thickness is incommensurate with the morphological layering distance. We estimate the average grain size using the orientational correlation length (ξ), computed using previously reported image analysis methods applied to the SEM micrographs.[38,41] We note that this means of estimating the grain size is very conservative, as it includes both the effect of abrupt changes of in-plane orientation appearing at grain boundaries and more subtle meandering of the morphology within a morphologically connected region. For oven annealing, the grains grow with annealing time, following a power law of the form $\xi = At^{\alpha}$. Grain coarsening in BCP systems is dominated by the diffusion and annihilation of topological defects within the morphology. The prefactor A includes the temperature dependence of the grain-coarsening process, which is frequently assumed to be Arrhenius-like, with an activation energy related to the barrier for defects to combine. The exponent α can vary depending on the dimensionality of the system (*e.g.*, bulk *vs* thin film) since this affects the random diffusion of the defects,[46] and more generally can be thought of as a proxy for describing the dominant mechanism for grain growth.[47]

For identical thin films processed using LZA, remarkably large grain sizes form, especially considering the extremely short annealing times. An example is shown in Figure 2 of a film that experienced only 15 s of annealing, yet yields grains ~3× larger than the corresponding oven-annealed sample. Remarkably, even millisecond annealing is sufficient to yield relatively well-ordered materials. Figure 2c compares quantitatively the grain-growth kinetics for LZA and oven annealing, where it is evident that LZA can reduce the time required to achieve a given grain size by 3 orders of magnitude. The exponent of the scaling is markedly different for LZA *vs* oven annealing, suggesting that the LZA method is affecting the grain-growth mechanism, rather than simply multiplying grain-growth rates. (Exponents as high as α = 0.48 were observed for 420 nm films; refer to the SI for details.) Moreover, this larger exponent shows that the disparity between LZA and oven annealing grows larger with

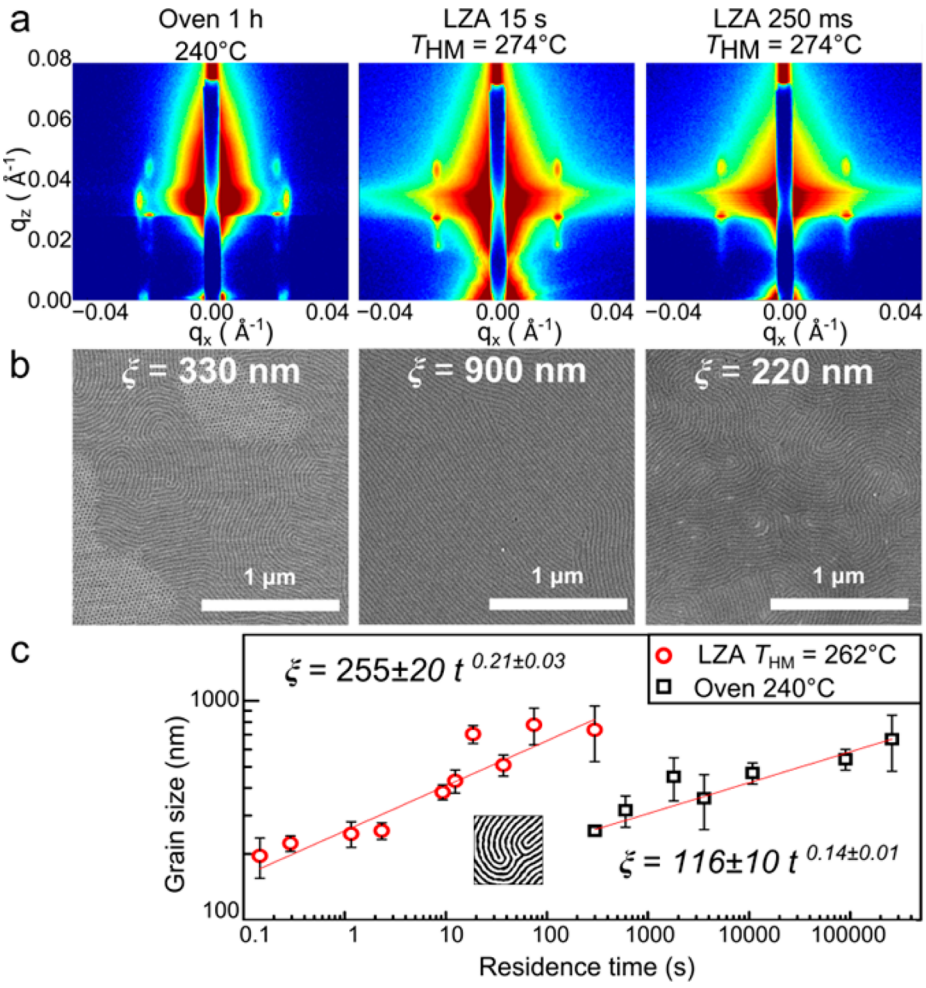

Figure 2. Accelerated kinetics of grain size development in LZA compared with conventional oven annealing. (a) GISAXS patterns and (b) corresponding SEM images of 170 nm thick PS-*b*-PMMA films annealed in the oven at 240 °C for 1 h and laser annealed for 15 s (T_{HM} = 274 °C); the latter yields grain sizes ~3× as large as oven annealing. Well-developed morphology can be obtained with LZA even after only 250 ms. (c) Evolution of grain size (horizontal cylinders) in an oven at 240 °C (black squares) and in LZA (red circles). Error bars represent the standard deviation obtained by analyzing different film regions. In LZA performed at constant sweep velocity, the width of the thermal field and the number of passages determine the effective annealing time. The data were fitted to a power law equation: red lines.

longer annealing times; the LZA method will always generate quantitatively better ordering if annealing is performed for sufficiently long. Experimentally, we observed that mere seconds of local annealing is sufficient to achieve the levels of order that are commonly targeted for BCP research.

For the film thickness studied here (170 nm), the morphology adopts a vertical cylinder orientation at early annealing times, but eventually converts to a horizontal orientation, passing through a coexistence region. Compared to oven annealing, LZA reduces the time scale for this reorientation by ~3 orders of magnitude (Figure 3), demonstrating that LZA enhances morphological conversion, in addition to grain coarsening.

Part of the enhancement of LZA must come from the high temperatures; for example, for annealing at T_{HM} = 262 °C, the film experiences a maximum temperature of 500 °C, albeit for an infinitesimal time. Because of the exponential dependence of grain growth rate on temperature, the short pulse of high-temperature annealing can yield substantial ordering. It is important to note, however, that LZA improves upon conventional oven annealing in that it exploits this high-temperature annealing without giving rise to film degradation. For conventional oven annealing, film degradation arises whenever the annealing temperature is too high (polystyrene degrades[48] at 330 °C, and poly(methyl methacrylate) at[49] 350 °C). Thermal polymer degradation is a stochastic process, influenced by exogenous species, and can thus accumulate even at lower temperatures if annealing times are sufficient. This limits the annealing times and temperatures that can be realistically used and thus limits the level of order possible for self-assembling materials. By comparison, LZA allows for substantial enhancement of the kinetics of morphological ordering, without simultaneously enhancing the kinetics of polymer degradation.[50]

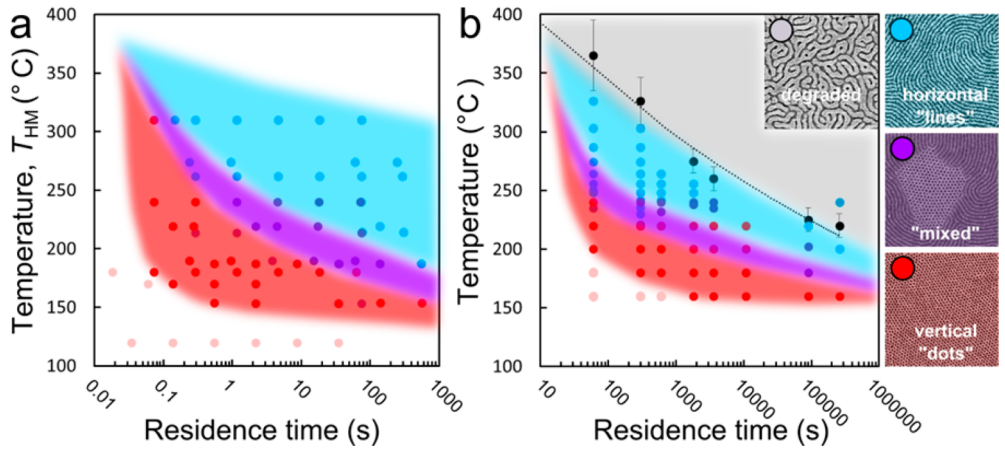

Figure 3. SEM morphology evolution of cylindrical domains in 170 nm thick PS-*b*-PMMA films. (a) LZA allows block copolymer film processing in less than a second without thermal degradation. (b) In conventional vacuum oven annealing, long processing times are required since excessively high temperatures lead to polymer degradation. Color legend: blue, horizontally oriented cylinders; red, vertical cylinders; violet, mixed morphology; gray, thermal degradation. Orientations were determined by SEM and confirmed by select GISAXS measurements.

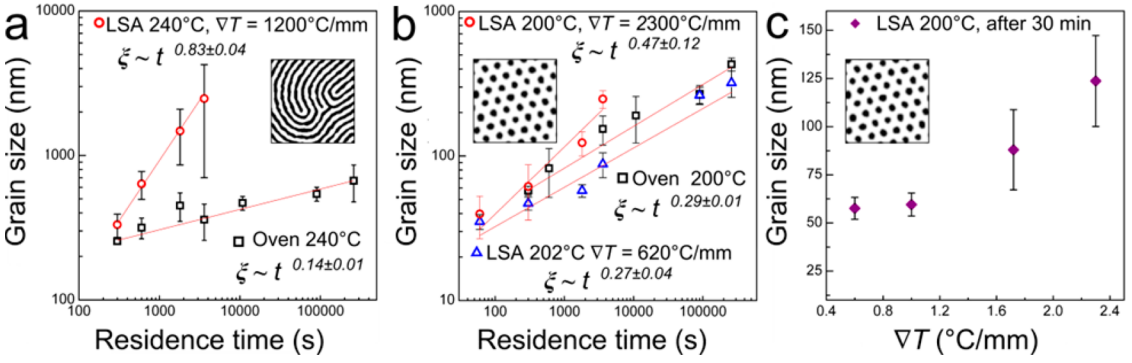

Figure 4. Enhancement of the grain-coarsening kinetics by temperature gradients. To facilitate direct comparison between laser and oven processing, the samples were subjected to laser static annealing (LSA), where a stationary laser line was heating the film, enabling unambiguous determination of annealing temperature (to within ±5 °C). (a) The time exponent of grain growth of horizontal morphology at ∇T = 1200 °C/mm (red dots) is much larger than for oven annealing at a matching temperature (black squares). (b) The influence of thermal gradients on growth kinetics of vertical (hexagonally packed) cylinders at 200 °C (∇T = 620 °C/mm, red circles; ∇T = 2300 °C/mm, blue triangles; oven, black squares). Data at longer times were obtained by analyzing the subregions exhibiting vertical orientation in mixed-morphology samples. (c) The grain size for vertical domains (30 min LSA at 200 °C) shows directly the influence of temperature gradient.

Indeed, we determined that LZA with extremely slow push speeds yields degradation, at rates quantitatively consistent with that observed for oven annealing (Figure 3b). This implies that zone annealing influences kinetics at the scale of the morphology, but is not accelerating molecular reactions or chain dynamics.

The high temperatures of LZA alone cannot explain the observed grain growth. Extrapolating oven annealing data to very high temperature (even ignoring the onset of polymer degradation) would not predict the rapid grain growth observed in LZA; indeed the increased exponent α observed for LZA suggests an alteration of the ordering mechanism. In order to isolate the thermal gradient contribution from the high-temperature contribution, we performed a series of laser static annealing (LSA) experiments, wherein the film was held stationary in the laser field. Different thermal histories (temperature and gradient) can be studied simply as a function of position within this static thermal field of a known profile. Figure 4 compares LSA data with corresponding oven annealing data (∇T = 0 °C/mm), for both horizontal cylinders (a) and vertical cylinders (b). Comparing matched temperatures, it is clear that annealing in the presence of a thermal gradient leads to faster grain growth. The effect of the gradient (relative increase in α) is more pronounced for the horizontal morphology than for the vertical morphology; this could suggest that the effect of the thermal gradient occurs at the scale of the morphology (*i.e.*, the BCP repeat spacing or larger). Morphological defects may be implicated; they can be thought of as quasi-particles arising from the collective behavior of many chains and whose size is determined by the repeat spacing. Increasing the thermal gradient (Figure 4c) systematically increases grain-coarsening rates. We propose that the strong thermal gradient

induces a thermophoretic force on the defects themselves, driving them toward the high-temperature end of the gradient (to lower the system free energy; refer to the SI). The concentration of defects would increase their annihilation rate, while being driven preferentially into the *higher* temperature region would simultaneous increase their diffusion speed and again increase annihilation probability. The thermophoretic driving of defects opens a more efficient defect annihilation mechanism and thus faster grain growth kinetics. The extremely large gradients available *via* photothermal fields are a particularly powerful way of exploiting this enhancement effect. Under this hypothesis, the thermal gradient is influencing the quasi-particle defects in the morphology, altering their diffusion without altering the diffusion or dynamics of the polymer chains.

With respect to the annealing times of LZA, Figure 5 shows a matrix of X-ray scattering data for combinations of sweep velocity and number. Annealing generates vertical cylinders (in-plane peaks in grazing-incidence small-angle X-ray scattering, GISAXS), which convert into horizontal states (peaks above the Yoneda line), which then coarsen (peak sharpening). For conserved total annealing time (diagonals in Figure 5), grain size is also conserved, except at very high sweep velocity (Figure 5b). Although laser power remains constant, rapid motion of the sample counteracts local heat buildup (Figure 5c). This effect could be offset by simply increasing the input laser power. However, our data indicate that there is no significant difference between slow and fast LZA processing, as long as the total residence time is conserved. Thus, although the spatial thermal gradient plays a critical role, it appears that the temporal thermal gradient does not. Finally, we note that even extremely short annealing times can, if accumulated, give rise to reasonable order. In other words, the BCP material is able to respond to thermal ordering on a millisecond time scale.

LZA demonstrably enhances ordering kinetics by orders of magnitude compared to oven annealing. However, processing a macroscopic sample with zone annealing involves translating the entire length of the sample through the narrow hot zone (*i.e.*, the laser line in LZA). Remarkably, the kinetic enhancement of LZA is more than sufficient to offset this. The *total* processing time for LZA (in contrast to the *local* annealing time, previously discussed) is dependent on the sample size (specifically, the sample length divided by the sweep velocity). For instance, at a sweep speed of 20 μm/s (and fwhm = 93 μm), the local annealing time is 5 s, while the total annealing time for a 1 cm sample would be 8 min. Since LZA can operate at sweep speeds of $\sim 10^3$ μm/s, the one-dimensional hot zone can process $\sim$1 mm of material per second; for example, a typical 1 cm sample can be entirely processed within $\sim$10 s. Thus, even over macroscopic areas, LZA can order material in record time (seconds to minutes). As another point of comparison, a vacuum oven has the advantage that it can process multiple samples simultaneously, limited by the size of the oven. LZA can, less conveniently, process samples in parallel, limited by the width of the laser line orthogonal to the sweep direction. Another possibility would be to generate a comb of laser lines (*e.g. via* interference) to induce multiple annealing cycles in a single sweep, thereby increasing throughput and offsetting the serial nature of LZA.

The ability of LZA to generate high temperatures over short time scales allows access to ordering regimes not seen in other techniques. In LZA, the annealing temperature can be adjusted using laser power or the thickness of the light-absorbing Ge layer or by tuning the temperature of the sample-mounting block. Figure 6a shows a sample processed using high-temperature LZA (T_{HM} = 312 °C), where spontaneous uniaxial alignment of the BCP morphology is observed over the macroscopic dimensions of the processed sample (see SI Figure S9). This "monodomain" global alignment yields effectively infinite grain size, from the point of view of the orientational correlation length. Thus, the previously described enhancement is a lower bound to the kinetic speedup that LZA can induce; high-temperature LZA yields grain sizes that diverge to infinity. This new phenomenon can be ascribed to local shear and flow of the polymer film (along the sweep direction), due to the high temperatures and the extreme thermal gradient. We confirm this hypothesis by processing samples with intentional discontinuities in the polymer film, where we observe (Figure 6b,c) that the morphology aligns along the local stress-relief direction; that is, creep-flow of the polymer causes the morphology to align perpendicular to the edges of the film (refer to SI Figure S10 for additional examples).

The use of a laser beam as a heat source offers a major advantage over conventional annealing techniques: it can be highly localized by the use of optical masking. More generally, an arbitrary pattern of thermal gradients can be induced by appropriate spatial and temporal control of the input light field. This points toward the tantalizing possibility of using LZA to simultaneously order and pattern materials. Here, we demonstrate several proofs-of-principle in this regard. First, we performed LZA through an optical mask, thereby spatially dictating annealing and thus patterning the morphology (refer to SI Figure S11). The size scale of this patterning is regulated by thermal diffusion; for the substrates studied here, this generates feature sizes of $\sim$70 μm or greater, with morphological-transition boundaries of width $\sim$4 μm. The results of Figure 6b,c provide a second demonstration. High-temperature LZA induces local BCP alignment that is regulated by the local stress-relief direction, *i.e.*, perpendicular to film boundaries. This allows relatively

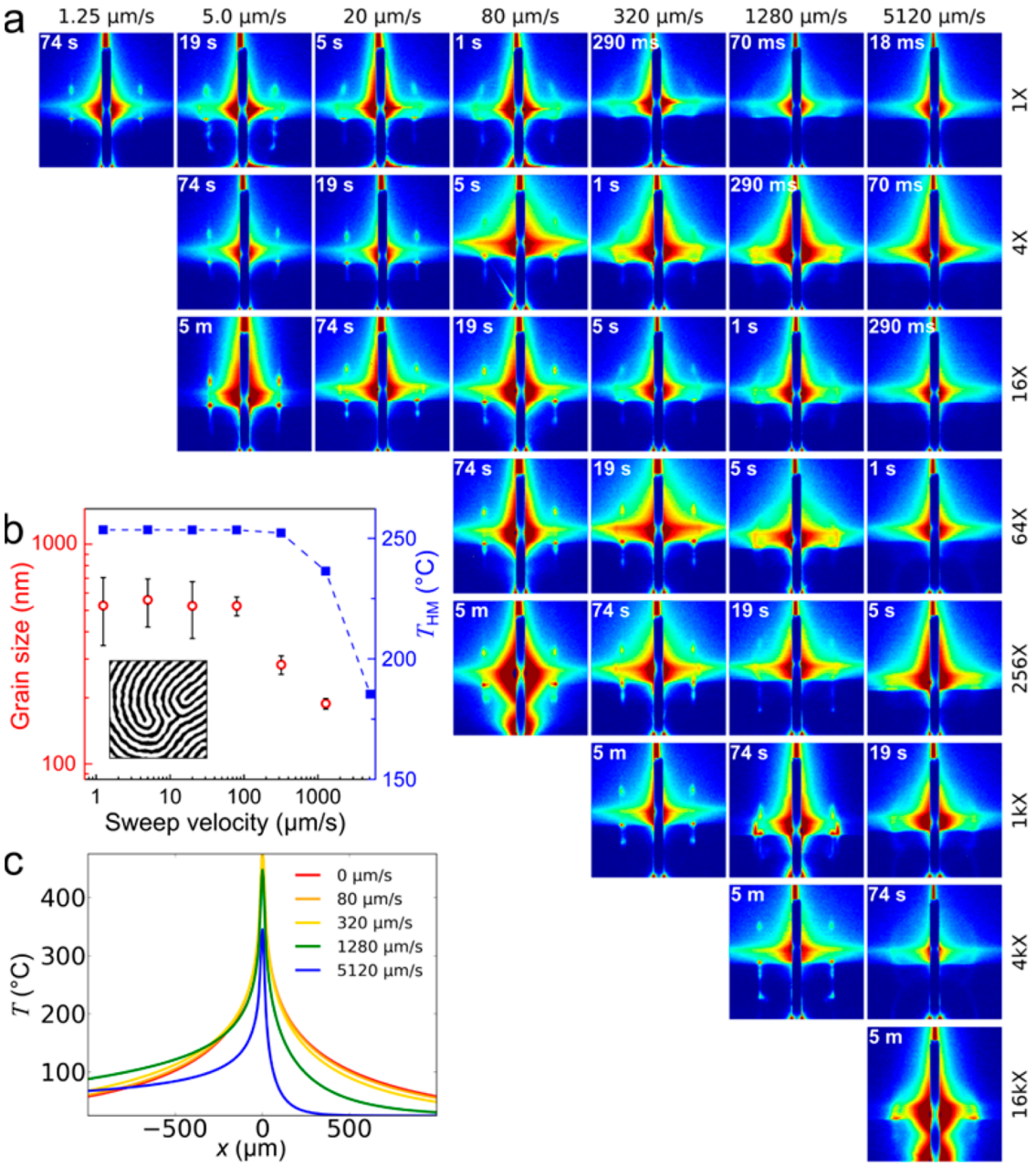

Figure 5. Influence of laser sweep velocity and number of sweeps on morphology of block copolymer films. (a) Synchrotron GISAXS patterns of 170 nm thick PS-*b*-PMMA on 100 nm Ge coated substrates. The progression along diagonals (upper-left to lower-right) corresponds to a constant total annealing time. Processing conditions: T_{HM} = 214 °C, fwhm = 93 μm. Complementary SEM images are presented in the SI. (b) The size of horizontal domains (red circles) with conserved total annealing time is unaffected by the sweep velocity below a critical value of ~300 μm/s. Above that velocity, substrate motion leads to substantial thermal transport away from the heated zone, lowering the processing temperature (blue squares) but sharpening the thermal profiles (shown in c), which decreases the annealing time. (c) Numerically simulated steady-state temperature profiles of substrates moved across the laser line at different velocity. Parameters used in the simulation were derived from experimentally obtained static temperature profiles.

coarse (microscale) structuring of the film continuity to template the nanoscale in-plane orientation of the morphology (see also SI Figure S10).

We can also activate shear effects at more modest temperatures by exploiting a soft polymer (polydimethylsiloxane, PDMS) capping layer on the BCP film during LZA processing. This "soft-shear" (SS) effect has been previously reported in conventional zone annealing experiments,[51] where the differential thermal expansion of the soft cladding (340 μm/m·K) compared to the rigid substrate (~8 μm/m·K) shears the polymer film. Figure 7 demonstrates that LZA can efficiently exploit this effect, aligning the morphology along the sweep direction. GISAXS indicates complete ordering through the film thickness (Figure 7c); uniaxial alignment was confirmed by the disappearance of the GISAXS peaks upon in-plane rotation (SI Figure S13). This near-perfect uniaxial alignment over

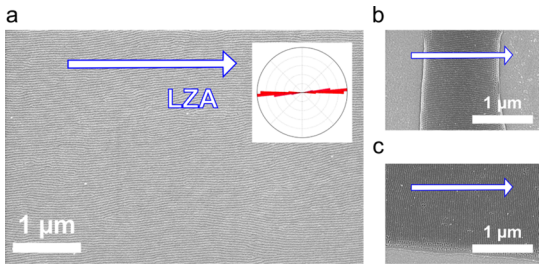

Figure 6. Uniaxial alignment induced by high-temperature LZA. (a) Performing LZA experiments at increased temperature (T_{HM} = 312 °C) accesses a new regime of ordering, where the sample is spontaneously aligned along the sweep direction (speed 20 μm/s), over the macroscopic dimensions of the sample (inset shows in-plane orientation histogram). This results from creep-flow of the film due to the transient high temperatures. (b) Discontinuities in the film surface can be used to locally align the morphology in-plane, since the material flows (and thus shears) along the perpendicular to an edge. (c) This is confirmed by using a film edge that is perpendicular to the sweep direction.

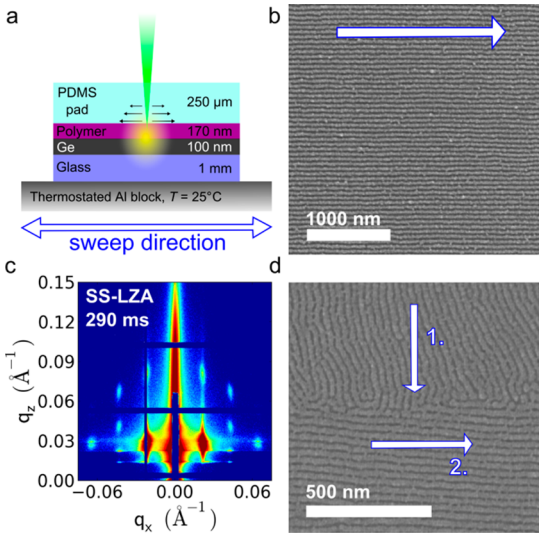

Figure 7. Soft-shear laser zone annealing (SS-LZA). (a) The shear effects of zone annealing can be enhanced by placing a PDMS pad on top of the polymer film. The large thermal expansion coefficient of PDMS induces a tangential stress in the film, along the laser sweep direction. (b) SEM micrograph of the surface of a film (170 nm) processed using a single sweep at 320 μm/s (laser line fwhm = 93 μm). The sample is uniformly aligned over the entire sample area (~400 mm^2). (c) GISAXS pattern collected after ultrafast SS-LZA processing reveals an exceptionally well-ordered block copolymer morphology aligned along the sweep direction. The image was collected with an X-ray beam along the sweep direction (refer also to the SI). (d) Example of local patterning with SS-LZA. A perpendicular junction pattern was obtained using two subsequent orthogonal laser sweeps with the use of a beam-masking edge.

macroscopic areas represents a degree of ordering impossible in conventional thermal annealing; yet LZA allows this exceptional order to be achieved within <300 ms. The localizable nature of LZA, coupled to SS, provides a third proof-of-principle with respect to patterning: an edge of the PDMS cladding can define a boundary between ordered/aligned material and disordered material. Figure 7d shows the formation of a right-angle contact line between two horizontal-cylinder domains. For this demonstration, the laser line was first swept over a film partially covered by a PDMS layer (the uncovered portion of the film was protected from light exposure using an optical mask). This laser passage creates a region of aligned BCP cylinders covering the exposed region, sharply terminated by the edge where illumination was blocked. During a second orthogonal laser sweep, the whole film is illuminated. However, the second aligned morphology is induced only in the previously unexposed region, since the domains are relatively stable against shear realignment. Figure 7d shows a magnified SEM image of the transition region between the two patterned zones (see SI Figure S12 for a larger view). The alignment direction on either side of the transition can be independently controlled by the sweep direction in the two SS-LZA steps. The boundary over which the alignment of the cylindrical domains shifts is locally very narrow (~$2L_0$), while its position at larger scales is determined by mask quality/alignment.

With respect to orientation control, Figures 6 and 7 demonstrate how LZA can exploit shear effects to control in-plane orientation of BCP morphology, while Figure 3 demonstrates how out-of-plane orientation can be controlled *via* annealing temperature and time. We note that this latter effect arises from the temperature-dependent surface tensions of PS and PMMA and may not generalize to all BCP materials.[7] On the other hand, the wide temperature range accessible to LZA may allow the exploitation of this effect in a wider range of materials. We also note that the morphological repeat spacing (L_0) is also temperature-dependent,[52,53] offering another way to tune material response. In particular, when film thickness is incommensurate with L_0, there is an energy penalty associated with horizontal alignment of the morphology, which can result in reorientation or the formation of surface terracing ("islands and holes").[4,54] For the results presented here (170 nm film thickness), we do not observe surface terracing. LZA experiments across a range of polymer film thicknesses displayed trends qualitatively matching those described for 170 nm films. Coupling LZA with commensurability effects is an exciting avenue for future study.

CONCLUSIONS

In conclusion, we have demonstrated that moving photothermal gradients can reduce the time required for ordering thin films of block copolymers. The high peak temperatures, coupled to extreme in-plane thermal gradients, allow grain growth kinetics to be enhanced by many orders of magnitude, without the onset of polymer degradation. Moreover, coupling to shear effects allows macroscopic uniaxial alignment of the block copolymer morphology in less than one second.

Mechanistically, we observe a kinetic enhancement for both grain growth and the kinetics of morphological reorientation. The grain-growth enhancement is different for horizontal and vertical morphologies. Taken together, our results may suggest that zone annealing operates at the scale of the morphology, not by affecting molecular/chain dynamics (indeed polymer degradation appears not to be enhanced). LZA alters the exponent of grain growth (α), which implies that it alters the mechanism of defect annihilation. The prefactor for grain growth (A) is also influenced by LZA (though more weakly), suggesting an alteration of the activation energy and/or frequency of defect annihilation. We propose that the spatial gradients are applying thermophoretic forces to the morphology, concentrating defects, and thereby increasing the rate of defect annihilation.

Our new technique has obvious advantages with respect to ordering kinetics. The enhanced scaling indicates that for sufficiently long annealing time, LZA will always exceed oven annealing in terms of grain size. For the materials and conditions studied here, this scaling is steep enough that even seconds of photothermal zone annealing can yield larger grains than hours of conventional oven annealing. Moreover, the orientation of the BCP morphology can be controlled with LZA, either through appropriate control of processing conditions (material-dependent) or by coupling to shear effects. Finally, LZA provides substantial control over the annealing process. Laser power allows control of temperature, while laser focus can tune the thermal gradient. The total annealing time can be controlled *via* the speed and number of sweeps. More generally, by controlling the incident light field, the ordering of the BCP can be prescribed in a spatially defined way. In other words, one can pattern at a micrometer scale using light, while allowing the BCP self-assembly to spontaneously produce the desired nanoscale pattern. Combined, these advantages poise photothermal zone annealing for providing rapid and robust control of block copolymer assembly in thin films.

METHODS

Polymer Film Preparation. Block copolymer films (170 nm thick) of cylinder-forming, polystyrene-*b*-poly(methyl methacrylate) (31.6−17.5 kg/mol, PDI = 1.06, Polymer Source) were prepared by spin-casting 3% toluene solutions onto germanium-coated (100 nm, Ar plasma-sputtered) 1 mm thick glass slides. Films were dried under vacuum at 60 °C for 4 h to remove residual solvent.[55] This BCP material exhibits a repeat spacing (cylinder-to-cylinder distance) of 31 nm when oven-annealed at 220 °C.

Oven Annealing. A reference set of samples (using identical substrates) was prepared in a vacuum oven with a temperature stability of ±3 °C, verified by independent thermocouple measurements.

Laser Annealing. A high-power (3 W) solid-state 532 nm green laser (Melles Griot 85 GHS 309) was used to irradiate the Ge-coated substrates. The beam was focused into a narrow (fwhm 20−400 μm) line (length ∼20 mm) at the film surface, using two spherical and one cylindrical lens. Beam width was tuned by adjusting the position of the first focusing lens. A holder supporting the substrates was placed inside a vacuum chamber fitted with a transparent quartz window (see Figure 1) attached to a motorized motion stage (Newport ILS 250CC). Optical profiles were measured by scanning a thermal power meter (Newport 70268) equipped with a 15 μm pinhole at the sample position. For laser annealing, the stage was swept across the laser line at velocities ranging from 1 to 5000 μm/s. If multiple sweeps were performed, the stage was moved across the beam in both directions. Laser power was controlled by inserting neutral density filters into the beam path.

Surface Temperature Profiling. A thin layer (∼200 nm) of a thermometric substance, tetrabutylammonium hexafluorophosphate (TBAHFP), an ionic compound with high melting point (245 °C), was spin-coated onto our glass/Ge substrates, yielding continuous films composed of very fine, submicrometer-sized crystallites. The films were vacuum-dried at 100 °C for 2 h before exposing them to a static laser beam. The film region heated above the melting point of TBAHFP becomes visually distinct, owing to dewetting and migration of film material. We refer to the resultant opening as a "melt-mark". The boundary of the melt-mark is an isotherm contour corresponding to 245 °C. Lowering the laser power narrows the melt-mark and allows extrapolation to temperatures higher than the melting point of TBAHFP using the formula

$$T_{EXT} = \frac{P_0}{P_{RED}}(T_{mp} - 25°C)$$

where T_{EXT}, P_{RED}, and P_0 are the extrapolated temperature, reduced laser power, and initial laser power, respectively. Conversely, lower isotherms were plotted using stearic acid (T_{mp} = 70 °C). The series of melt-marks allows reconstruction of the full experimental thermal profile due to the laser line. We observed excellent agreement between our experimental thermal profile and the analytical prediction (further details in the SI), validating our method. The results are further corroborated using our previously described numerical simulation.[56] These simulations are used to predict the temperature profiles that exist during laser/substrate motion, *i.e.*, the dynamic temperature fields that arise in LZA sweeps.

Soft-Shear LZA. Polydimethylsiloxane (Sylgard 184 with 5:1 mix ratio) precursor was cast onto Petri dishes to a thickness of ∼300 μm and cured under vacuum at 80 °C for 24 h. The PDMS pads were cut and transferred onto the polymer films, where intimate surface adhesion was observed. The samples were laser annealed as previously described. After the annealing the pads were gently peeled off; no evidence of residual PDMS was observed on the BCP films.

Morphology Characterization. The surface morphology of samples was characterized, after acetic acid removal of the PMMA block, using scanning electron microscopy (Hitachi S-4800). High-resolution (2560 × 1920 pixels) images at a magnification of 25 000× were used for grain size analysis. We use the orientational correlation as an estimate of the grain size, as previously reported.[38,41] Briefly, particle analysis was used to differentiate between film regions of horizontal morphology (larger image structures consistent with "lines") and vertical morphology (small structures consistent with hexagonally packed "dots"). For the horizontal regions, spatial derivatives were used to compute a local in-plane orientation map, whereas for vertical morphologies vectors between nearest neighbors were used to compute the average local in-plane orientation of the hexagons. The orientational correlation function was then calculated using

$$g(r) = \langle \psi(0)\, \psi(r) \rangle$$

where the angled brackets denote averaging over all angles for a given distance r. Finally, a correlation length, ξ, was computed by fitting $g(r)$ to an exponential decay function, $e^{-r/\xi}$. An average value of the correlation length was obtained from at least five micrographs.

GISAXS. Grazing-incidence small-angle X-ray scattering measurements were performed at the X9 beamline of the National Synchrotron Light Source at Brookhaven National Laboratory. Samples were measured under vacuum using an X-ray beam of 13.5 keV (λ = 0.0918 nm). GISAXS data presented were collected across a range of incidence angles (0.07° to 0.20°). Silver behenate powder was used as a standard for data conversion to q-space.

Conflict of Interest: The authors declare no competing financial interest.

Acknowledgment. Research was carried out at the Center for Functional Nanomaterials and the National Synchrotron Light Source, Brookhaven National Laboratory, which are supported by the U.S. Department of Energy, Office of Basic Energy Sciences, under Contract No. DE-AC02-98CH10886.

Supporting Information Available: Supporting Information provides details of LZA setup, temperature profiling (surface thermometry) method, and grain-size analysis. Additional experimental results are presented, including SEM images of oven- and LZA-processed films, films aligned using high-temperature and soft-shear LZA, and films ordered by patterning through an optical mask or using sequences of soft-shear processing. We also present a simple thermophoretic model. This material is available free of charge *via* the Internet at http://pubs.acs.org.

REFERENCES AND NOTES

1. Bates, F. S.; Fredrickson, G. H. Block Copolymer Thermodynamics: Theory and Experiment. *Annu. Rev. Phys. Chem.* **1990**, *41*, 525–557.
2. Fasolka, M. J.; Mayes, A. M. Block Copolymer Thin Films: Physics and Applications. *Annu. Rev. Mater. Res.* **2001**, *31*, 323–355.
3. Bates, C. M.; Maher, M. J.; Janes, D. W.; Ellison, C. J.; Willson, C. G. Block Copolymer Lithography. *Macromolecules* **2013**, *47*, 2–12.
4. Albert, J. N. L.; Epps, T. H. Self-Assembly of Block Copolymer Thin Films. *Mater. Today* **2010**, *13*, 24–33.
5. Mansky, P.; Russell, T. P.; Hawker, C. J.; Mays, J.; Cook, D. C.; Satija, S. K. Interfacial Segregation in Disordered Block Copolymers: Effect of Tunable Surface Potentials. *Phys. Rev. Lett.* **1997**, *79*, 237.
6. Huang, E.; Rockford, L.; Russell, T. P.; Hawker, C. J. Nanodomain Control in Copolymer Thin Films. *Nature* **1998**, *395*, 757.
7. Han, E.; Stuen, K. O.; Leolukman, M.; Liu, C.-C.; Nealey, P. F.; Gopalan, P. Perpendicular Orientation of Domains in Cylinder-Forming Block Copolymer Thick Films by Controlled Interfacial Interactions. *Macromolecules* **2009**, *42*, 4896–4901.
8. Sivaniah, E.; Hayashi, Y.; Iino, M.; Hashimoto, T.; Fukunaga, K. Observation of Perpendicular Orientation in Symmetric Diblock Copolymer Thin Films on Rough Substrates. *Macromolecules* **2003**, *36*, 5894–5896.
9. Ho-Cheol, K.; Charles, T. R.; Linnea, S. Fabrication of 20nm Half-Pitch Gratings by Corrugation-Directed Self-Assembly. *Nanotechnology* **2008**, *19*, 235301.
10. Park, S.; Lee, D. H.; Xu, J.; Kim, B.; Hong, S. W.; Jeong, U.; Xu, T.; Russell, T. P. Macroscopic 10-Terabit-per-Square-Inch Arrays from Block Copolymers with Lateral Order. *Science* **2009**, *323*, 1030–1033.
11. Pereira, G. G.; Williams, D. R. M. Diblock Copolymer Melts in Electric Fields: The Transition from Parallel to Perpendicular Alignment Using a Capacitor Analogy. *Macromolecules* **1999**, *32*, 8115–8120.
12. Ashok, B.; Muthukumar, M.; Russell, T. P. Confined Thin Film Diblock Copolymer in the Presence of an Electric Field. *J. Chem. Phys.* **2001**, *115*, 1559–1564.
13. Osuji, C.; Ferreira, P. J.; Mao, G.; Ober, C. K.; Vander Sande, J. B.; Thomas, E. L. Alignment of Self-Assembled Hierarchical Microstructure in Liquid Crystalline Diblock Copolymers Using High Magnetic Fields. *Macromolecules* **2004**, *37*, 9903–9908.
14. Koppi, K. A.; Tirrell, M.; Bates, F. S. Shear-Induced Isotropic-to-Lamellar Transition. *Phys. Rev. Lett.* **1993**, *70*, 1449.
15. Riise, B. L.; Fredrickson, G. H.; Larson, R. G.; Pearson, D. S. Rheology and Shear-Induced Alignment of Lamellar Diblock and Triblock Copolymers. *Macromolecules* **1995**, *28*, 7653–7659.
16. Angelescu, D. E.; Waller, J. H.; Adamson, D. H.; Deshpande, P.; Chou, S. Y.; Register, R. A.; Chaikin, P. M. Macroscopic Orientation of Block Copolymer Cylinders in Single-Layer Films by Shearing. *Adv. Mater.* **2004**, *16*, 1736–1740.
17. Davis, R. L.; Chaikin, P. M.; Register, R. A. Cylinder Orientation and Shear Alignment in Thin Films of Polystyrene−Poly(N-Hexyl Methacrylate) Diblock Copolymers. *Macromolecules* **2014**, *47*, 5277–5285.
18. Segalman, R. A.; Hexemer, A.; Kramer, E. J. Effects of Lateral Confinement on Order in Spherical Domain Block Copolymer Thin Films. *Macromolecules* **2003**, *36*, 6831–6839.
19. Sundrani, D.; Darling, S. B.; Sibener, S. J. Guiding Polymers to Perfection: Macroscopic Alignment of Nanoscale Domains. *Nano Lett.* **2003**, *4*, 273–276.
20. Hammond, M. R.; Cochran, E.; Fredrickson, G. H.; Kramer, E. J. Temperature Dependence of Order, Disorder, and Defects in Laterally Confined Diblock Copolymer Cylinder Monolayers. *Macromolecules* **2005**, *38*, 6575–6585.
21. Yang, X. M.; Peters, R. D.; Nealey, P. F.; Solak, H. H.; Cerrina, F. Guided Self-Assembly of Symmetric Diblock Copolymer Films on Chemically Nanopatterned Substrates. *Macromolecules* **2000**, *33*, 9575–9582.
22. Ouk Kim, S.; Solak, H. H.; Stoykovich, M. P.; Ferrier, N. J.; de Pablo, J. J.; Nealey, P. F. Epitaxial Self-Assembly of Block Copolymers on Lithographically Defined Nanopatterned Substrates. *Nature* **2003**, *424*, 411.
23. Cheng, J. Y.; Ross, C. A.; Smith, H. I.; Thomas, E. L. Templated Self-Assembly of Block Copolymers: Top-Down Helps Bottom-Up. *Adv. Mater.* **2006**, *18*, 2505–2521.
24. Ruiz, R.; Kang, H.; Detcheverry, F. A.; Dobisz, E.; Kercher, D. S.; Albrecht, T. R.; de Pablo, J. J.; Nealey, P. F. Density Multiplication and Improved Lithography by Directed Block Copolymer Assembly. *Science* **2008**, *321*, 936–939.
25. Bita, I.; Yang, J. K. W.; Jung, Y. S.; Ross, C. A.; Thomas, E. L.; Berggren, K. K. Graphoepitaxy of Self-Assembled Block Copolymers on Two-Dimensional Periodic Patterned Templates. *Science* **2008**, *321*, 939–943.
26. Yang, J. K. W.; Jung, Y. S.; Chang, J.-B.; Mickiewicz, R. A.; Alexander Katz, A.; Ross, C. A.; Berggren, K. K. Complex Self-Assembled Patterns Using Sparse Commensurate Templates with Locally Varying Motifs. *Nat. Nanotechnol.* **2010**, *5*, 256–260.
27. Chang, J.-B.; Choi, H. K.; Hannon, A. F.; Alexander-Katz, A.; Ross, C. A.; Berggren, K. K., Design Rules for Self-Assembled Block Copolymer Patterns Using Tiled Templates. *Nat. Commun.* **2014**, *5*.
28. Welander, A. M.; Kang, H.; Stuen, K. O.; Solak, H. H.; Müller, M.; de Pablo, J. J.; Nealey, P. F. Rapid Directed Assembly of Block Copolymer Films at Elevated Temperatures. *Macromolecules* **2008**, *41*, 2759–2761.
29. Maher, M. J.; Bates, C. M.; Blachut, G.; Sirard, S.; Self, J. L.; Carlson, M. C.; Dean, L. M.; Cushen, J. D.; Durand, W. J.; Hayes, C. O.; Ellison, C. J.; Willson, C. G. Interfacial Design for Block Copolymer Thin Films. *Chem. Mater.* **2014**, *26*, 1471–1479.
30. Kimura, M.; Misner, M. J.; Xu, T.; Kim, S. H.; Russell, T. P. Long-Range Ordering of Diblock Copolymers Induced by Droplet Pinning. *Langmuir* **2003**, *19*, 9910–9913.
31. Seppala, J. E.; Lewis, R. L.; Epps, T. H. Spatial and Orientation Control of Cylindrical Nanostructures in Aba Triblock Copolymer Thin Films by Raster Solvent Vapor Annealing. *ACS Nano* **2012**, *6*, 9855–9862.

32. Sinturel, C.; Vayer, M.; Morris, M.; Hillmyer, M. A. Solvent Vapor Annealing of Block Polymer Thin Films. *Macromolecules* **2013**, *46*, 5399–5415.
33. Zhang, X.; Harris, K. D.; Wu, N. L. Y.; Murphy, J. N.; Buriak, J. M. Fast Assembly of Ordered Block Copolymer Nanostructures through Microwave Annealing. *ACS Nano* **2010**, *4*, 7021–7029.
34. Pfann, W. G. Zone Melting: This Technique Offers Unique Advantages in Purification and in Control of Composition in Various Substances. *Science* **1962**, *135*, 1101–1109.
35. Lovinger, A. J.; Chua, J. O.; Gryte, C. C. Studies on the α and β Forms of Isotactic Polypropylene by Crystallization in a Temperature Gradient. *J. Polym. Sci., Part B: Polym. Phys.* **1977**, *15*, 641–656.
36. Hashimoto, T.; Bodycomb, J.; Funaki, Y.; Kimishima, K. The Effect of Temperature Gradient on the Microdomain Orientation of Diblock Copolymers Undergoing an Order-Disorder Transition. *Macromolecules* **1999**, *32*, 952–954.
37. Bodycomb, J.; Funaki, Y.; Kimishima, K.; Hashimoto, T. Single-Grain Lamellar Microdomain from a Diblock Copolymer. *Macromolecules* **1999**, *32*, 2075–2077.
38. Berry, B. C.; Bosse, A. W.; Douglas, J. F.; Jones, R. L.; Karim, A. Orientational Order in Block Copolymer Films Zone Annealed below the Order-Disorder Transition Temperature. *Nano Lett.* **2007**, *7*, 2789–2794.
39. De Rosa, C.; Park, C.; Thomas, E. L.; Lotz, B. Microdomain Patterns from Directional Eutectic Solidification and Epitaxy. *Nature* **2000**, *405*, 433.
40. Angelescu, D. E.; Waller, J. H.; Adamson, D. H.; Register, R. A.; Chaikin, P. M. Enhanced Order of Block Copolymer Cylinders in Single-Layer Films Using a Sweeping Solidification Front. *Adv. Mater.* **2007**, *19*, 2687–2690.
41. Yager, K. G.; Fredin, N. J.; Zhang, X.; Berry, B. C.; Karim, A.; Jones, R. L., Block-Copolymer Ordering through a Moving Thermal Zone. *Soft Matter* **2010**, DOI: 10.1039/B916200C.
42. Yager, K. G.; Barrett, C. J. All-Optical Patterning of Azo Polymer Films. *Curr. Opin. Solid State Mater. Sci.* **2001**, *5*, 487–494.
43. Singer, J. P.; Kooi, S. E.; Thomas, E. L. Focused Laser Spike (Flask) Annealing of Photoactivated Chemically Amplified Resists for Rapid Hierarchical Patterning. *Nanoscale* **2011**, *3*, 2730–2738.
44. Jung, B.; Ober, C. K.; Thompson, M. O.; Chandhok, M. Lwr Reduction and Flow of Chemically Amplified Resist Patterns during Sub-millisecond Heating. *SPIE Adv. Lithogr.* **2011**, *7972*, 79722S–79722S-8.
45. Singer, J. P.; Gotrik, K. W.; Lee, J.-H.; Kooi, S. E.; Ross, C. A.; Thomas, E. L. Alignment and Reordering of a Block Copolymer by Solvent-Enhanced Thermal Laser Direct Write. *Polymer* **2014**, *55*, 1875–1882.
46. Harrison, C.; Adamson, D. H.; Cheng, Z.; Sebastian, J. M.; Sethuraman, S.; Huse, D. A.; Register, R. A.; Chaikin, P. M. Mechanisms of Ordering in Striped Patterns. *Science* **2000**, *290*, 1558–1560.
47. Vega, D. A.; Harrison, C. K.; Angelescu, D. E.; Trawick, M. L.; Huse, D. A.; Chaikin, P. M.; Register, R. A. Ordering Mechanisms in Two-Dimensional Sphere-Forming Block Copolymers. *Phys. Rev. E* **2005**, *71*, 061803.
48. Malhotra, S. L.; Hesse, J.; Blanchard, L.-P. Thermal Decomposition of Polystyrene. *Polymer* **1975**, *16*, 81–93.
49. Ferriol, M.; Gentilhomme, A.; Cochez, M.; Oget, N.; Mieloszynski, J. L. Thermal Degradation of Poly(Methyl Methacrylate) (PMMA): Modelling of Dtg and Tg Curves. *Polym. Degrad. Stab.* **2003**, *79*, 271–281.
50. Our choice of temperature metric is arbitrary, but we note that comparison between Figure 3a and b, in particular the upper limits before degradation, supports this as being a fair metric. By studying the order at the thermal front itself (LSA experiments), we confirmed that even the center of the hot zone is not in fact driving the BCP through the order−disorder transition temperature.
51. Singh, G.; Yager, K. G.; Berry, B.; Kim, H.-C.; Karim, A. Dynamic Thermal Field-Induced Gradient Soft-Shear for Highly Oriented Block Copolymer Thin Films. *ACS Nano* **2012**, *6*, 10335–10342.
52. Hashimoto, T.; Shibayama, M.; Kawai, H. Ordered Structure in Block Polymer Solutions. 4. Scaling Rules on Size of Fluctuations with Block Molecular Weight, Concentration, and Temperature in Segregation and Homogeneous Regimes. *Macromolecules* **1983**, *16*, 1093–1101.
53. Mansky, P.; Tsui, O. K. C.; Russell, T. P.; Gallot, Y. Phase Coherence and Microphase Separation Transitions in Diblock Copolymer Thin Films. *Macromolecules* **1999**, *32*, 4832–4837.
54. Forrey, C.; Yager, K. G.; Broadaway, S. P. Molecular Dynamics Study of the Role of the Free Surface on Block Copolymer Thin Film Morphology and Alignment. *ACS Nano* **2011**, *5*, 2895–2907.
55. Zhang, X.; Yager, K. G.; Kang, S.; Fredin, N. J.; Akgun, B.; Satija, S.; Douglas, J. F.; Karim, A.; Jones, R. L. Solvent Retention in Thin Spin-Coated Polystyrene and Poly(Methyl Methacrylate) Homopolymer Films Studied by Neutron Reflectometry. *Macromolecules* **2009**, *43*, 1117–1123.
56. Yager, K. G.; Barrett, C. J. Temperature Modeling of Laser-Irradiated Azo-Polymer Thin Films. *J. Chem. Phys.* **2004**, *120*, 1089–1096.